Journal homepage www. jzs.uos.edu.krd
Journal of Zankoi Sulaimani
Part-A- (Pure and Applied Sciences)

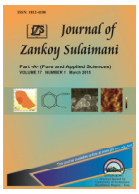

Enhancement efficiency of P3HT:PCBM solar cell by different treatment annealing

Abdullah A. Hussein[1], Waleed A. Hussain[2], Hussein F. Al-luaiby[2], Tamara Basova[3]& Aseel K. Hassan[4]

1 Department of Material Science, Polymer Research Centre, University of Basrah,
2 Department of physics, college of education, Basrah University
3 Nikolaev Institute of Inorganic Chemistry SB RAS, Novosibirsk, 630090, Russia
4 Materials and Engineering Research Institute, Sheffield Hallam University, Sheffield S1 1WB, UK

e.mail: amanar_2005@yahoo.com

Article info

Original: 11 Nov. 2014
Revised: 03 Dec. 2014
Accepted: 10 Dec. 2014
Published online:
20 March 2015

Key Words:
Solvent vapor annealing-
Post annealing
P3HT:PCBM
nanoparticle

Abstract

Solvent Vapor Annealing (SVA) followed by Post Thermal Annealing (SVA-PA) are demonstrated as attractive methods to anneal polymer blend films and represent a very useful process to control the morphology for high performance polymer solar cells (PSCs). It is found that compared with general annealing processes, the crystallinity of regioregular poly (3-hexylthiophene) (rr-P3HT) has enhanced by performing SVA-PA on freshly deposited films. In this work we have investigated thin film blend produced from P3HT and [6,6]-phenyl-C61 butyric acid methylester (PCBM) materials. This photoactive layer is sandwiched between an anode composed of indium tin oxide (ITO)/poly(3,4 ethylenedioxythiophene):poly(styrene sulfonate) (PEDOT:PSS) gold nanoparticles (AuNPs) and Al as the cathode layer. Atomic force microscopy (AFM) study reveals that the SVA annealed films exhibit smooth surface and homogenous conductivity distribution. Moreover, an enhanced light harvesting and increased crystallinity of P3HT in the active layer are observed by UV–vis absorption and X-ray diffraction (XRD). We have seen that thermal annealing significantly improves the optical absorption ability for all treatment. We have also the current density- voltage characteristics and External quantum efficiency (EQE) of different thermal annealing.

Introduction

Polymer solar cells (PSCs) have attracted considerable interest over the last two decades due to their unique advantages which include low processing cost, lightweight, mechanical flexibility, potential for large-scale fabrication and versatility of chemical structure [1,2]. Recently high Power Conversion Efficiency (PCE) of about 8% has been reported for devices based on bulk heterojunction (BHJ) of donor-acceptor materials [3-5]. Significant work was focused on the use of polymeric systems comprising poly (3-hexylthiophene):[6,6]-phenyl C61- butyric acid methyl ester (P3HT:PCBM) blends for the fabrication of BHJ solar cells [6–9].
Different treatments of such blends have been examined to tailor the morphology of the layer, and thus enhancing their photovoltaic properties. Several approaches have been proposed in order to manipulate the phase separation in these nanostructured films which include post-deposition thermal annealing (where the polymer film is heated above its glass transition or melting temperature) [10,11], the use of mixed solvents (co-solvent, where a high-boiling-point solvent is mixed with a low-boiling-point solvent) [12,13], slow growth [14,15] and solvent vapor annealing [16–18]. It is worth mentioning that solvent vapor annealing has been exploited due to its versatility to the dissolvable π-conjugated polymers, as well as the associated low processing cost of large areas. Furthermore, solvent vapor annealing is a room temperature, which could

prevent degradation of thermally sensitive materials compared with thermal annealing approach [19–21]. It has been extensively used in organic electronics, such as organic thin film transistors (OTFTs), light emitting diodes (LED) and Polymer Solar Cells (PSCs), in which the crystallinity or structure order of the films has significantly improved device performance [22,23].

Extensive efforts have been devoted to establish general methods of self-assembly and self-organization through intermolecular interaction of π-conjugated molecules [22]. It is well known that improved morphology with nanoscale interpenetrating network could enhance device efficiency through performing annealing treatment of active films. As a solution-assisted method, solvent vapor annealing (SVA), which takes place via exposing films of functional materials to an environment saturated with solvent vapors, proved to be an effective room temperature treatment in triggering self-assembly and thus enhancing the crystal order of organic semiconductors [23]. The solvent vapor and the thin condensed solvent layer on the substrates provide a medium for re-crystallization [23-28]. There have been significant studies of solvent vapor annealing-post annealing (SVA-PA) on inorganic substrates and it has been shown that the recrystallization or long-range self-assembly of semiconductor molecules can be assisted by an appropriate selection of substrate surface [26,27].

In this work, we have investigated the effect of thermal annealing on the performance, crystallinity and the interface morphology of polymer solar cells by applying different annealing sequences; these are, post-annealing (PA), solvent annealing only (SVA) and solvent vapor annealing followed by post annealing (SVA-PA) and we have compared the performance and morphologies of these devices with un-annealed (UA) samples. We have also incorporated thin film of gold nanoparticles (AuNPs) as an anode buffer layer to increase the PEDOT:PSS conductivity. The AuNPs are used due to the strong local electric field caused by surface plasmons can enhance the exciton dissociation in OPVs contributing positively to power conversion. Furthermore recent studies demonstrated that the NPs can lead to an enhancement of the OPV device structural stability as well.

Experiment

A. Photovoltic device fabrication

Pre-patterned indium tin oxide (ITO)-coated glass slides (80 nm in thickness and 25 Ω/sq sheet resistance, Sigma-Aldrich) were used as substrates and to act as transparent anode contact. The ITO-coated slides were first ultrasonicated in acetone and in isopropyl alcohol for 10 min, and finally heat- dried in an oven at 120 ^{o}C. The gold nanoparticles AuNPs (5nm diameter, Sigma-Aldrich) were added to linear polystyrene (PS) in order to inhibit the dewetting in the spun-cast films [10]. The PS acts as an inert host to improve the film forming property of the AuNPs [10]. The AuNPs solution was prepared by mixing the AuNPs with the PS (1:4 w/w) using toluene as solvent. A film of poly(3,4-ethylenedioxythiophene) poly (styrenesulfonate) (PEDOT:PSS:AuNPs) was spun onto the ITO substrates with a spin speed of 2000 rpm for 40 s to form the hole- transport layer, and was dried for 15 min at 140 ^{o}C. Afterwards, mixed solutions consisting of conjugate polymer P3HT (10 mg mL^{-1}, Sigma-Aldrich) and PCBM fullerene (`10mgmL^{-1}, Sigma-Aldrich) , 1:1 weight ratio, are prepared in a co-solvent consisted of chlorobenzene and chloroform (CB:CF) in 1:1 weight ratio. The obtained polymer blend (P3HT:PCBM) solutions were spun onto the PEDOT:PSS film at 800 rpm for 30s to form the active layer. The thickness of the active layer is ~150 nm and that of the PEDOT:PSS layer is 30 nm, both measured using spectroscopic ellipsometry. Finally, a cathode consisting of 100 nm Al was thermally evaporated under vacuum of ~ 2×10^{-5} Pa with a rate of deposition of 0.2 nm/s onto the active layer surface. The devices produces have an active area of 9 mm^2 defined by the shadow mask used to deposit the cathode. Solvent Vapor Annealing (SVA) was carried out by directly placing the substrates with the active layer facing the solvent-filled petri dishes for 5 h at 125 ^{o}C. In Post Thermal Annealing (PTA) process, the produced devices were placed on a hot plate at 125 °C for 15 min. Solvent Vapor Annealing followed by Post Thermal Annealing (SVA-PTA) was carried out by performing SVA for 5 h followed by PTA for 15 min at 125 ^{o}C. The cathode was already deposited onto the active layer prior to all annealing processes.

B. Device characterization

The current density-voltage (J-V) characteristics of the fabricated devices (device structure is described in Fig.1(b) were measured with a computer-controlled Keithley 6517A digital source meter and the photocurrent was generated under AM 1.5G irradiation source of 100 mWcm^{-2}. A bias voltage is swept typically from -0.1V to +0.1 V with a step of 10 *mV*. The mounting table and the spring probe pins with magnetic bases were designed and constructed in the lab. P3HT:PCBM (molecular structures are given in Fig.1(a) films were prepared by spin coating their solution in CB:CF co-solvent on glass substrates for UV-vis absorption spectroscopy and onto Si substrates (10x10 mm^2) for atomic force microscopy (AFM). The UV-vis absorption spectra of the polymer films were recorded on Varian 50 scan UV-visible spectrophotometer and Raman spectra were measured using a Renishaw RM2000 confocal Raman microprobe system , including a Renishaw RM1000 NIR 780TF diode laser (wavelength 514 nm) with a maximum output power of 25 mW. (Al substrate was used for the Raman spectroscopy measurements). The AFM images of the polymer films were acquired using a BRUKER NanoScope IV Multi-Mode Adapter AFM with the tapping mode. The blend structures were investigated by multipurpose X'Pert PHLIPS X-Ray defractometer (MPD), and the film thickness was determined using M2000V (J.A. Woollam Co., Inc.) spectroscopic ellipsometer, operating in the wavelength range 370-1000 nm.

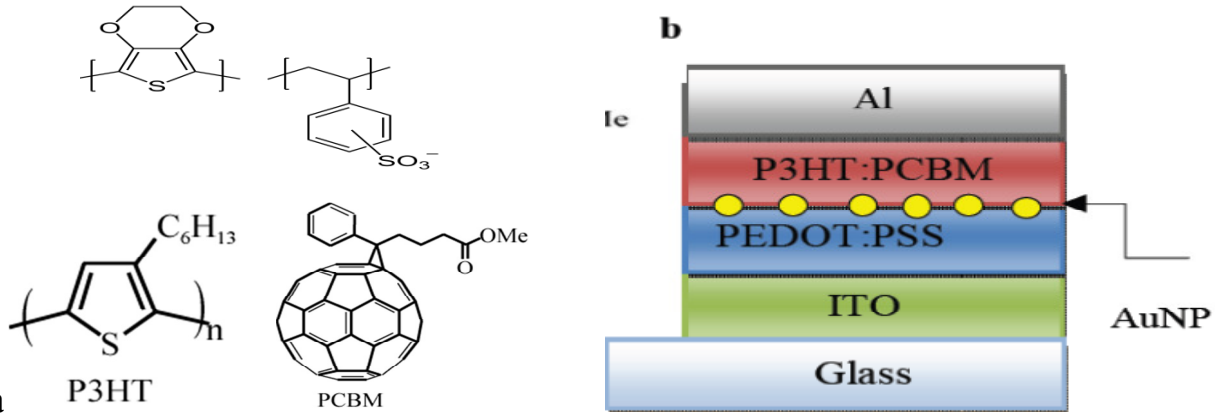

Fig.1.(a) Molecular structures of PEDOT:PSS: AuNPs/P3HT:PCBM, (b) photovoltaic device structure.

The photoconversion efficiency η was determined using the following relation:

$$\eta = FF \times (V_{oc} \times J_{sc})/P_{light} \qquad (1)$$

where the FF is the fill factor and is defined as :

$$FF = (I_{max} \times V_{max})/(I_{sc} \times V_{oc}) \qquad (2)$$

V_{oc} is the open-circuit voltage, J_{sc} the short circuit current density, and the P_{light} is the power of incident light. In Eq. (2) I_{max} and V_{max} are the current and voltage at the maximum power point.
In this work, We extracted the I-V data from measurement three similar devices.

Results and Discussion:

Solvent vapor annealing followed by post thermal annealing has been proven to be a useful process to improve the power conversion efficiency of (ITO/PEDOT: PSS:AuNPs/P3HT:PCBM/Al) device solar cells [30]. The optical absorption spectra of P3HT/PCBM films, before (UA) and after (PA, SVA and SVA-PA) treatment, are shown in Fig. 2. It is clearly shown that annealing treatments lead to an increase in absorption intensity in the range from 400 nm to 600 nm. This can be ascribed to the increased π-π* interaction of the P3HT molecules with increased chain ordering [30,31]. Furthermore, the development of vibronic shoulders (~610 nm) corresponds to the enhanced inter-chain stacking ordering in the P3HT clusters [32]. It is worthwhile mentioning that the PCBM absorption peak (~330 nm) has also increased as a result of post deposition treatment. It has been reported in the literature that thermal annealing as well as various other post

deposition treatments have not resulted in significant changes in the absorption peak of PCBM [31,33]. Our results however imply that the SVA and SVA-PA not only increases the P3HT molecular stacking and ordering but also induces PCBM cluster formation.

An appropriate PCBM clustering process was reported to enhance the PV performance due to formation of pathways for charge transport [34].

Figure 3 shows the XRD patterns for the as-deposited and annealed blend films. A characteristic (100) peak around $2\theta=5.4^{o}$ representing the oriented edge-on P3HT crystallites with the lamella structure of thiophene rings in P3HT [34] has grown up significantly with SVA, PA and SVA-PA respectively, and its half width has decreased. This indicates the increase in the degree of crystallization and/or the grain size of P3HT domains by annealing treatment. The SVA and PA annealed films show a reduced intensity of (100) peak as compared to that of the SVA-PA annealed film. The lowest crystallinity was observed for the as deposited (un-annealed) film. We assume that the presence of PCBM molecules affect the structure of P3HT crystallites at room temperatures. Upon annealing (PA and SVA-PA), the significant increase in P3HT crystallinity can be ascribed to the full self-assembly of the conjugated chain leading to the orderly formed and increased length of the conjugated bond. This is due to the increased thermal diffusion of PCBM molecules at elevated temperatures to form larger PCBM aggregates [35,36,37]. As a result, regions with low PCBM concentration will occur. In these regions with low PCBM concentration (phase-separated networks), the P3HT aggregates form larger crystallites and thus facilitates charge transport to the electrodes [38].

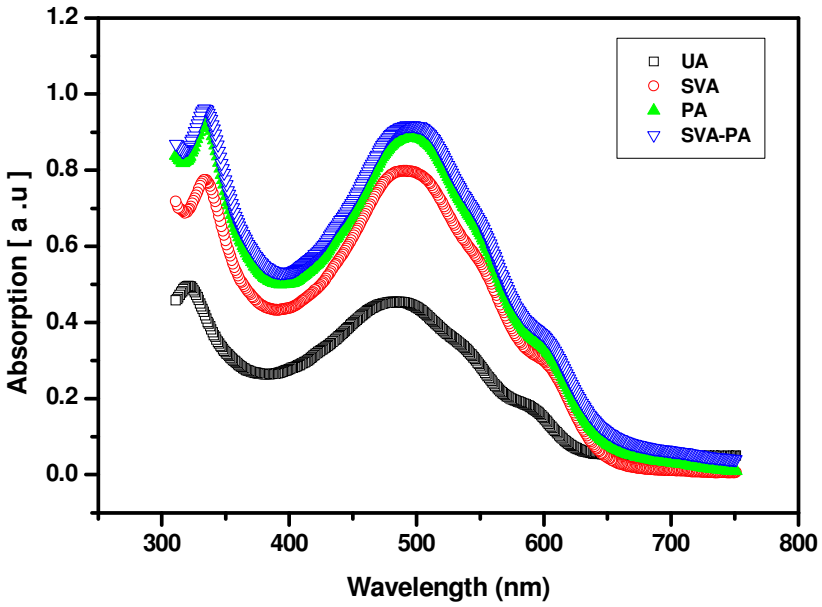

Fig.2. UV–vis absorption spectra for PEDOT:PSS: AuNPs/P3HT:PCBM thin films by UA, SVA, PA and SVA-PA.

The solar cell device active layer (P3HT/PCBM blend) was characterized by Raman spectroscopy in the range 200-2000 cm^{-1}. There are several Raman modes in the range 600-1600 cm^{-1} [39, 40]: the main in-plane ring skeleton modes at 1452 cm^{-1} (symmetric C=C stretching mode) and at 1380 cm^{-1} (C-C intra-ring stretching mode), the inter-ring C-C stretching mode at 1208 cm^{-1}, the C-H bending mode with the C-C inter-ring stretch mode at 1180 cm^{-1}, and the C-S-C deformation mode at 728 cm^{-1}.

We focus on the two main in-plane ring skeleton modes at ~1450 and ~1380 cm^{-1} (Figure 4) because they are supposed to be sensitive to π-electron delocalization (conjugation length) of P3HT molecules [41] as well as to crystallinity extent [42, 43].

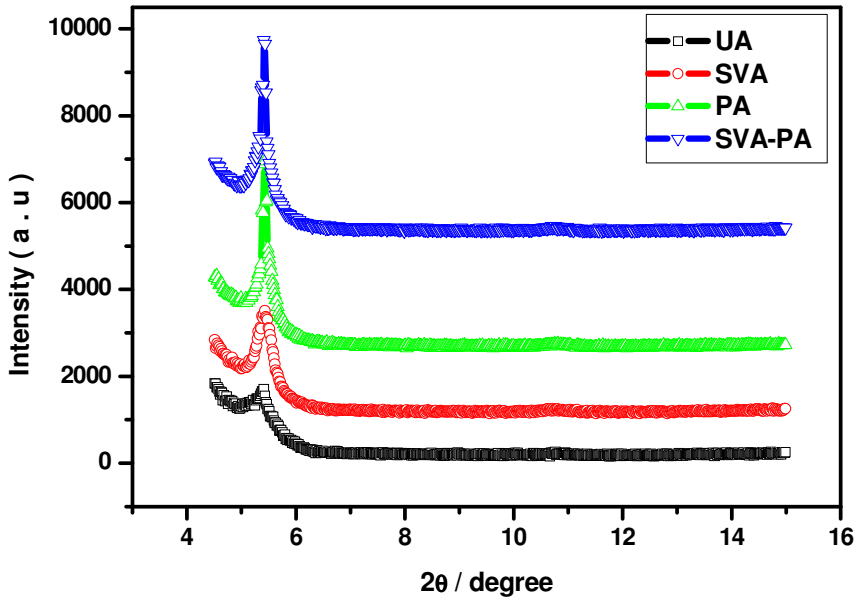

Fig.3. (XRD) curves for PEDOT:PSS:AuNPs /P3HT: PCBM thin films by UA, SVA, PA and SVA-PA.

As Figure 4 shows, noticeable changes can be observed in the main in-plane ring skeleton Raman modes characteristics upon annealing: (i) a shift to lower wavenumber in the C=C mode peak position (1452 cm^{-1} for UA film); (ii) a larger intensity of the C-C mode (1380 cm^{-1} for UA film) with respect to the C=C mode. Tsoi et al. [42] observed the same behavior of the Raman modes in thermal annealed P3HT:PCBM layers, which was attributed to a higher degree of P3HT crystallinity upon annealing. The maximal shift of 3 cm^{-1} was observed for SVA-PA film. A shift in the wavenumber generally indicates an increase in the crystallinity of P3HT polymer and the extension of the effective conjugation length along the polymer backbone [43]. This result agrees well with the XRD analysis.

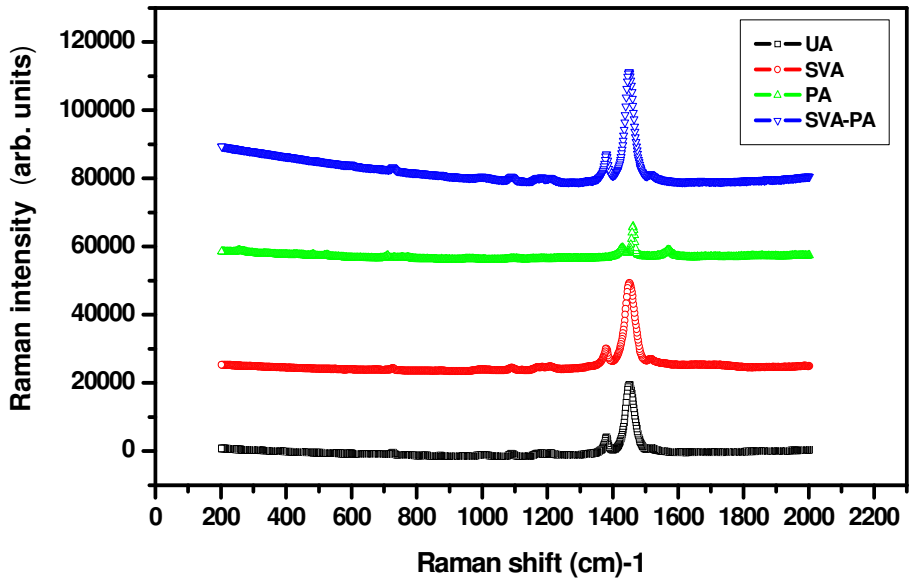

Fig.4. Raman spectra for PEDOT:PSS:AuNPs /P3HT:PCBM thin films by UA, SVA, PA and SVA-PA.

The bulk-heterojunction morphology (BHJ) of un-annealed and annealed films was investigated using atomic force microscopy (AFM). The as-deposited (UA) films exhibit a smooth surface, in which the phase separation is not obvious and the root-mean-square (R.M.S) roughness of the film is 2.6 nm, as shown in Fig.5(a). The SVA films exhibit a structured surface with more domains of the two components comprising the films. The distinct phase-separation appears due to sufficient time allowed for self-organization of P3HT (5h at 125^{o}C) resulting in R.M.S roughness of about 3.1 nm. The network between P3HT and PCBM domains has gradually formed. Figs. 5(c) and (d) show surface roughness of PA and SVA-PA treated films, respectively. For the PA treated devices (15 min at 125 °C) the interpenetrating networks are clearly demonstrated, as illustrated further in the schematic diagram in Fig 5.

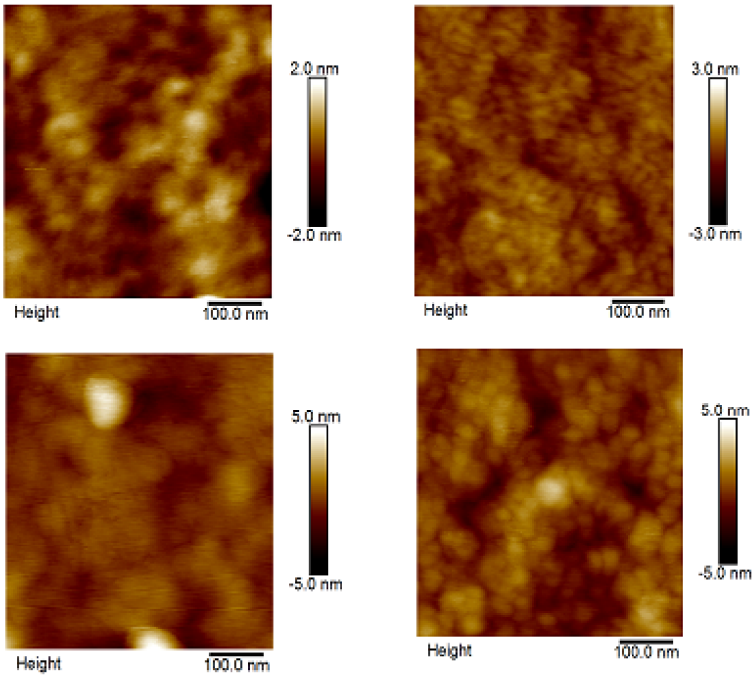

Fig. 5. AFM images of the (a) UA, (b) SVA, (c) PA and (d) SVA-PTA for PEDOT:PSS:AuNPs/P3HT :PCBM layers.

The surface of films subjected to SVA-PA treatment shows clear donor-accepter domains within the active layer, and the R.M.S roughness measured for PA and SVA-PA films increased from 3.21 nm to 3.31 respectively. Table 1 summarizes the films' parameters as obtained from AFM image analysis; R_a is the film's mean roughness, R_{max} the maximum height of the film and R.M.S is its root mean square roughness.

Table 1. AFM value for Photovoltaic properties of the UA, SVA, PA and SVA-PA.

Annealing	R.M.S (nm)	R_a(nm)	R_{max}(nm)
UA	2.60	2.04	19.9
SVA	3.09	2.49	23.2
PA	3.21	2.4	32
SVA-PA	3.31	2.45	32.5

External quantum efficiencies of the organic solar cells under different fabrication conditions annealing treatment are shown in Fig. 6. The curves of EQE essentially followed the absorption spectrum of the P3HT:PCBM active layer in the range about 350–650 nm corresponding to the absorption wavelength range of P3HT. Consistent with the tendency of *J*sc, curve (SVA-PA treated) displayed the highest EQE, while the curve (as-deposited) reference device had the lowest EQE, in the range 350–650 nm. And there are three vibronic absorption at λ= 520, 554 (peaks) and 650 (shoulder) nm in the visible region for the P3HT :PCBM

active layer except for the as-cast reference device (the peak at 512 nm is the absorption of P3HT main chain, and the other two peaks at longer wavelength are due to the interchain interactions in the ordered P3HT crystalline regions in the films). The more pronounced crystalline peaks of PA and SVA-PA treated processed films than the as-deposited reference film may also explain why the PA and SVA-PA processed devices exhibited a higher *J*sc [35,37].

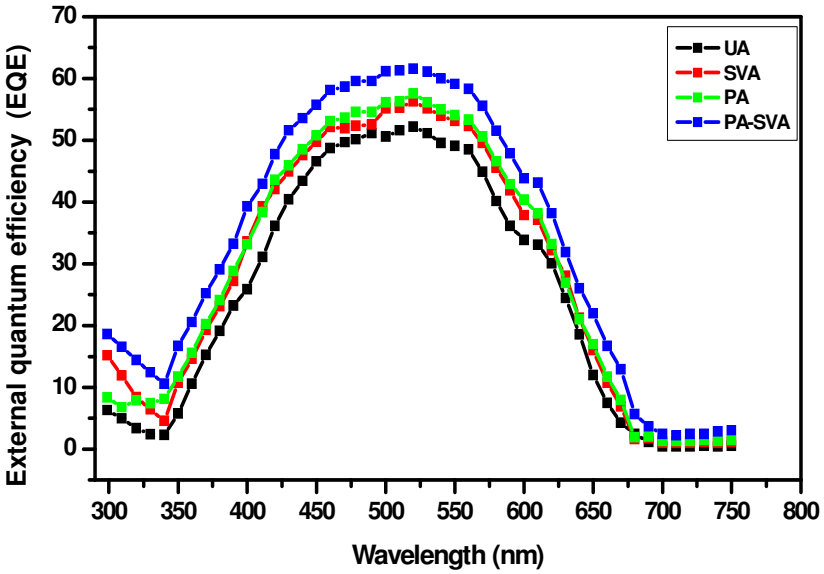

Fig.6. External quantum efficiency (EQE) spectra of PEDO:PSS:AuNPs /P3HT:PCBM films by (a) UA, SVA (b), PA (c) and(d) SVA-PA.

The current density (J) versus voltage (V) characteristics of the ITO/PEDOT:PSS: AuNPs/P3HT:PCBM/Al devices are presented in Fig. 7. The PV device parameters have been calculated using Eqs. (1) and (2) and are summarized in Table 2. The highest efficiency of 3.7% was obtained for the device which was subjected to solvent followed by thermal annealing (SVA/PTA) treatment while the lowest efficiency of 2.04% was associated with devices without any post deposition treatment. SVA-PA treated devices have exhibited larger I_{sc} vlaues of about 9.5 $mAcm^{-2}$ but with a V_{oc} value similar to those obtained for untreated as well as otherwise post-deposition treated devices. The increase in the device short circuit current can be explained by the increased roughness (R.M.S) of the polymer blend causing an increase in the contact area at the interface between the active layer and the Al cathode. This is thought to facilitate Al layer reshaping following the active layer surface morphology, and thus improving interfacial adhesion [44]. Furthermore, the rough active layer can trap light effectively thus increasing light absorption [45]. PA treatment at 125 °C for 15 min improves the interface between the cathode and active layer, and the nanoscale phase separation results in the improvement of PCE.

Table 2. Photovoltaic properties of the devices made with buffer layer and photoactive layer using 1:1ratio of P3HT to PCBM and gold nanoparticles.

Annealing	V_{oc}(v)	J_{sc}(mA/ cm^2)	FF	PCE(%)
UA	0.63	5.16	0.63	2.04
SVA	0.64	6.29	0.64	2.53
PA	0.65	6.72	0.64	2.79
SVA-PA	0.63	9.49	0.62	3.7

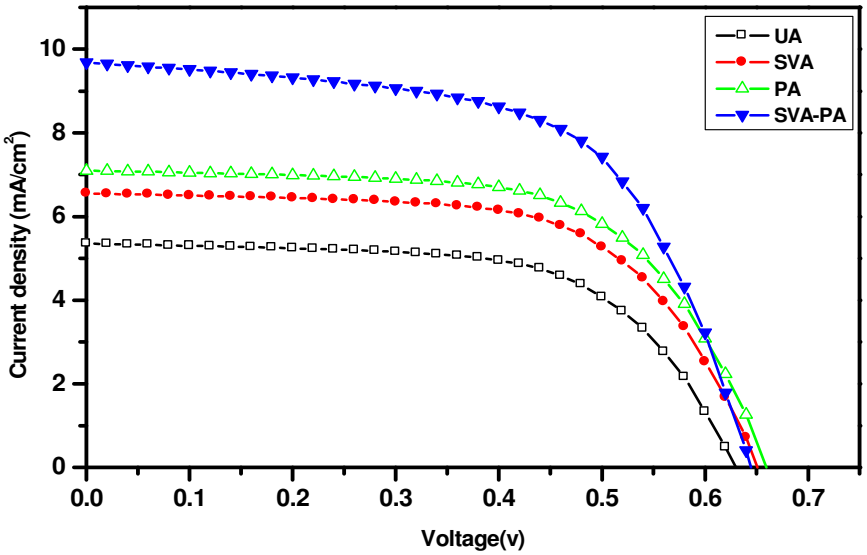

Fig.7. J–V characteristics for PEDOT:PSS:AuNPs/ P3HT:PCBM thin films by UA, SVA, PA and SVA-PA.

Conclusion

Organic solar cells with high efficiencies were fabricated using P3HT:PCBM: PEDOT:PSS:AuNPs structures. The inclusion of gold nanoparticles in PEDOT:PSS buffer layer is thought to enhance light harvesting for the OSCs of P3HT:PCBM. The effects of films' treatment by performing SVA, PA and SVA-PA on the performance of PSCs were investigated. The SVA-PA has been shown to improve the morphology and crystallinity of the films, and therefore enhance the PCEs of the devices. The advantages of the SVA-PA approach are more pronounced at higher PCBM loading. The variation in PCE is partially explained by the longer conjugation length and formation of a band structure in well-organized P3HT domains in solvent annealed solar cells. With subsequent thermal annealing, the solar cells upon (SVA-PA) give Power Conversion Efficiency (PCE) of 3.7%, in contrast to 2.79% for the post-annealed (PA), 2.53% for the Solvent Vapor Annealing (SVA) and 2.04% for the un-annealed (UA) devices.

Achnowledgment

This research work was supported by the University of Barsrah and by Materials and Engineering Research Institute, Sheffield Hallam University, Sheffield S11WB, UK.

Refrences

[1] H. Lv, X. Zhao, W Xu, H. Li, J. Chen, X. Yang, Organic Electronics 14 (2013) 1874–1881
[2] G. Li, R. Zhu, Y. Yang, Polymer solar cells, Nat. Photonics 6 (2012) 153–161.
[3] He Z., Zhong C., Huang X., Wong W.-Y., Wu H., Chen L., Su S. and Cao Y., Adv. Mater. 23, (2011) 4636.
[4] Zhou H., Yang L. and You W., Macromolecules 45, (2012) 607.
[5] Li X., Choy W. C. H., Huo L., Xie F., Sha W. E. I., Ding B., Guo X., Li Y., Hou J., You J. and Yang Y., Adv. Mater. 24, (2012) 3046.
[6] G. Li, V. Shrotriya, J. Huang, Y. Yao, T. Moriarty, K. Emery, Y. Yang, Nat. Mater., 4, (2005), 864.
[7] M. Reyes-Reyes, K. Kim, D. L. Carroll, Appl. Phys. Lett. 87, (2005) 083 506.
[8] G. Li, V. Shrotriya, Y. Yao, Y. Yang, J. Appl. Phys. , 98 (2005), 043 704.
[9] W. Ma, C. Yang, X. Gong, K. Lee, A. J. Heeger, Adv. Funct. Mater. , 15 (2005) 1617.

[10] T. Wang, A. J. Pearson, D. G. Lidzey, R. A. L. Jones, 21 (2011)1383–1390.
[11] N. D. Treat, C. G. Shuttle, M. F. Toney, C. J. Hawker, M. L. Chabinyc, Journal of Materials Chemistry,21(2011)15224–15234.
[12] Y. Yao, J. Hou, Z. Xu, G. Li, Y. Yang, Adv.Functional Mate., 18(2008) 1783–1789.
[13] B. Schmidt-Hansberg, M. Sanyal, N. Grossiord, Y. Galagan, M. Baunach, M.F.G. Klein, A. Colsmann, P. Scharfer, U. Lemmer, H. Dosch, J. Michels, E. Barrena, W. Schabel, Solar Energy Mater. .Solar Cells 96(2012)195–201.
[14]G. Li, Y. Yao, H. Yang, V. Shrotriya, G. Yang, Y. Yang, Adv.Functional Mater.17 (2007) 1636–1644.
[15] G. Wei, S. Wang, K. Sun, M. E. Thompson, S. R. Forrest, Adv. Energy Mater. 1 (2011)184–187.
[16] H. Tang, G. Lu, L. Li, J. Li, Y. Wang, X. Yang, J.. Mater. Chem.20 (2010) 683–688.
[17] T. A. Bull, L. S. C. Pingree, S. A. Jenekhe, D. S. Ginger, C. K. Luscombe, ACSNano3 (2009) 627–636.
[18] R. Hegde, N. Henry, B. Whittle, H.D. Zang, B. Hu, J.H. Chen, K. Xiao, M. Dadmun, Sol. Energy Mater. Sol. Cells 107 (2012) 112–124.
[19] G. de Luca, A. Liscio, P. Maccagnani, F. Nolde, L. M. Scolaro, V. Palermo, K. M€ullen and P. Samor, Soft Matter., 4 (2008), 2064.
[20] V. Palermo and P. Samor, Angew. Chem., Int. Ed. , 46 (2007) 4428.
[21] J. M. Mativetsky, M. Kastler, R. C. Savage, D. Gentilini, M. Palma, W.Pisula, K.M€ullen , P. Samor, Adv. Funct.Mater. , 19, (2009) 2486.
[22] A. Datar, R. Oitker and L. Zang, Chem. Commun., (2006), 1649.
[23] E. Treossi, A. Liscio, X. Feng, V. Palermo, K.M€ullen and P. Samor_ı, Small, 5(2009), 112.
[24] H.-Y. Chen, J.-L. Wu, C.-T. Chen, C.-T. Chen,. 48 (2012) 1012–1014.
[25] S. Miller, G. Fanchini, Y.-Y. Lin, C. Li, C.-W. Chen, W.-F. Su, M. Chhowalla, J. Mater. Chem. 18 (2008) 306–312.
[26] A. Amassian, V.A. Pozdin, R. Li, D.-M. Smilgies, G.G. Malliaras, J. Mater. Chem. 20 (2010) 2623–2629.
[27] A. L. Briseno, S. C. B. Mannsfeld, S. A. Jenekhe, Z. Bao and Y. Xia, Mater. Today, 11 (2008) 38.
[28] G. de Luca, A. Liscio, P. Maccagnani, F. Nolde, V. Palermo, K. M€ullen and P. Samor_ı, Adv. Funct. Mater., (2007), 17, 3791.
[29]M. J. Beliatis, S. J. Henley, S. Han, K. Gandhi, A. A. D. T. Adikaari,Z.E.Stratakis, E.Kymakis, S. R. P. Silva, Phys. Chem. Chem. Phys., 15, (2013) 8237
[30] T. F. Guo, T. C. Wen, G. L. Pakhomov, X. G. Chin, S.H. Liou , P. H. Yeh, C. H. Yang, Thin Solid Films, 516 (2008) 3138–3142.
[31] Y.C. Huang, Y.C. Liao, S.S. Li, M.C. Wu, C.W. Chen, W.F. Su, Solar Energy Materials and Solar Cells 93 (2009) 888–892.
[32] G. Li, V. Shrotriya, J. Huang, Y. Yao, T. Moriarty, K. Emery, Y. Yang, Nature Materials 4 (2005) 864–888.
[33] H.Y. Park, K. Kim, D.Y. Kim, S.K. Choi, S.M. Jo, S.Y. Jang, Journal of Materials Chemistry 21 (2011) 4457–4464.
[34] M.Y. Chiu, U.S. Jeng, C.H. Su, K.S. Liang, K.H. Wei, 20 (2008) 2573–2578.
[35] H. Hoppe, M. Niggemann, C. Winder, J. Kraut, R. Hiesgen, A. Hinsch, D. Meissner, N.S. Sariciftci, Adv. Funct. Mater. 14 (2004) 1005.
[36] D. Chirvase, J. Parisi, J.C. Hummelen, V. Dyakonov, Nanotechnology 15 (2004) 1317.
[37] X. Yang, J.K.J. van Duren, R.A.J. Janssen, M.A.J. Michels, J. Loos, Macromolecules 37 (2004) 2151.
[38] Ma W. L., Yang C. Y., Gong X., Lee K. and Heeger A. J., Adv. Funct. Mater. 15,1617 (2005).
[39] W.C. Tsoi, D. T. James, J. S. Kim, P. G. Nicholson, C. E. Murphy, D. D. C. Bradley, J. Nelson, J.-S. Kim, ǀJ. Am. Chem. Soc. 2011, 133, 9834–9843
[40] Baibarac, M.; Lapkowski, M.; Pron, A.; Lefrant, S.; Baltog, I. J. Raman Spectrosc. 1998, 29, 825–832.
[41] Gao, Y.; Gery, J. K. J. Am. Chem. Soc. 2009, 131, 9654–9662.

[42] Tsoi, W. C.; James, D. T.; Kim, J. S.; Nicholson, P. G.; Murphy, C. E.; Bradley, D. D. C.; Nelson, J.; Kim, J. S. J. Am. Chem. Soc. 2011, 133, 9834–9843

[43] G. Louarn, M. Trznadel, J.P. Buisson, J. Laska, A. Pron,M. Lapkowski, S.J. Lefrant, Phys. Chem. 100 (1996) 12532.

[44] Y. Xuan, Y.ming, H.yang, ZHANG Jian-jun, ZHAO Gengshen , Z. Ying. Optoelectron. Lett. 9.4 · (2013) 0275.

[45] Hu Z., Zhang J. and Zhao Y., Org. Electron. (2012) 13, 142.